J Appl Electrochem (2007) 37:439–449
DOI 10.1007/s10800-006-9274-0

ORIGINAL PAPER

# Surface and electrochemical characterization of pitting corrosion behaviour of 304 stainless steel in ground water media

**D. Gopi · S. Manimozhi · K. M. Govindaraju · P. Manisankar · S. Rajeswari**

Received: 4 June 2006 / Accepted: 27 October 2006 / Published online: 13 January 2007


**Abstract** The effectiveness of aminotrimethylidene phosphonic acid (ATMP) as a corrosion inhibitor in association with a bivalent cation like $Zn^{2+}$ and non-ionic surfactant like polyoxyethylene sorbitan monooleate (Tween 80) were investigated by measuring corrosion losses using electrochemical techniques. The corrosion of 304 stainless steel in the ground water medium was inhibited by complexation of the inhibitor. A combined inhibition effect was achieved by adding both ATMP and $Zn^{2+}$ along with Tween 80. The formulation functioned as a mixed type inhibitor. The synergistic effect of the inhibitor compound is calculated. Luminescence spectra, FTIR spectra, XRD, XPS and scanning electron microscopic studies were carried out to understand the mode of corrosion inhibition and also the morphological changes on the metal surface.

**Keywords** 304 Stainless steel · Pitting corrosion · Corrosion inhibition · Impedance · Surface characterization · XPS

D. Gopi (✉) · S. Manimozhi · K. M. Govindaraju · P. Manisankar
Department of Chemistry, Periyar University, Salem 636 011 Tamilnadu, India
e-mail: periyaruniversitygopi@yahoo.co.in

S. Rajeswari
Department of Analytical Chemistry, University of Madras, Guindy Campus, Chennai 600 025, India

## 1 Introduction

Scaling and corrosion control by the application of inhibitors is the most popular method. An abundance of literature concerning scaling and corrosion, as well as inhibition of corrosion of mild steel has been published [1–3]. Complex formation, interphase inhibition and surface micelle formation effects have been proposed for metals under uniform corrosion conditions [4–6] and such process may also be important for the inhibition of localized forms of attack on passive metals [7–14]. Electrochemical techniques have provided only macroscopic details of the redox reaction and no mechanistic information [15–24]. In order to gain a better understanding of the metal surface reaction for surface analytical techniques must be used [25–27]. Over the last two decades, significant advances have been made in applying surface-sensitive techniques in unraveling the chemical reaction on the metal surfaces in catalysis [28–30]. Most of these techniques can be readily used in the field of corrosion. It is expected that significant advances in the theoretical and practical understanding of the mechanisms of corrosion and corrosion inhibition will arise from the use of these surface analytical tools [31–37].

The aim of the present study was to investigate synergistic corrosion inhibition for the combination of aminotrimethylidene phosphonic acid (ATMP), $Zn^{2+}$ and Tween 80. The synergism was evaluated by OCP time measurements, potentiodynamic polarization and impedance measurements. The anti-corrosive passive film formed on the 304 SS was characterised with the help of surface analytical techniques such as Luminescence Spectra, Fourier Transform-Infrared Spectroscopy (FTIR), X-ray diffraction technique (XRD),

X-ray Photoelectron Spectroscopy (XPS) and Scanning Electron Microscopy (SEM).

## 2 Experimental

### 2.1 Electrochemical techniques

#### *2.1.1 Electrode preparation*

The composition of 304 SS used was Cr – 18%, Ni – 8%, C – 0.07%, Mn – 1.72%, Si – 1.03%, P – 0.039%, S – 0.016% and Fe-balance. The material was cut into pieces 1 × 1 × 0.3 cm in size for electrochemical studies. Each piece was attached with a brass rod using silver paste for electrical contact. Then the samples were mounted on an epoxy resin in such a way that only one side with 1 $cm^2$ surface area was exposed. The mounted samples were polished successively up to 1000 grit SiC emery paper and final polishing was done with 6 and 1 $\mu$m diamond paste. The samples were degreased with acetone and ultrasonically cleaned using deionized water. This served as the working electrode. Groundwater of composition given in Table 1 was used as the medium. Its conductivity of ground water is 1690 $\mu S\ cm^{-1}$. Electrochemical studies were carried out in a conventional three-electrode cell consisting of a platinum counter electrode, a saturated calomel reference electrode (SCE) and the working electrode.

#### *2.1.2 Open circuit potential measurement*

As soon as the samples were immersed in the electrolyte, the initial potentials of the samples were noted and monitored as a function of time until they reached a steady value. Similar experiments were carried out in the presence of the inhibitors, which were purchased from Aldrich Co Ltd. The structures of the inhibitor compounds are given in Fig. 1.

#### *2.1.3 Polarization measurement*

Polarization measurements were carried out using a Bio-Analytical system electrochemical analyzer (BAS).

**Table 1** Analysis of groundwater

| Species | Con./ppm |
|---|---|
| Total dissolved salts | 1185 |
| Total Alkalinity | 330 |
| Calcium | 131 |
| Magnesium | 43 |
| Chloride | 279 |
| Sulphate | 130 |

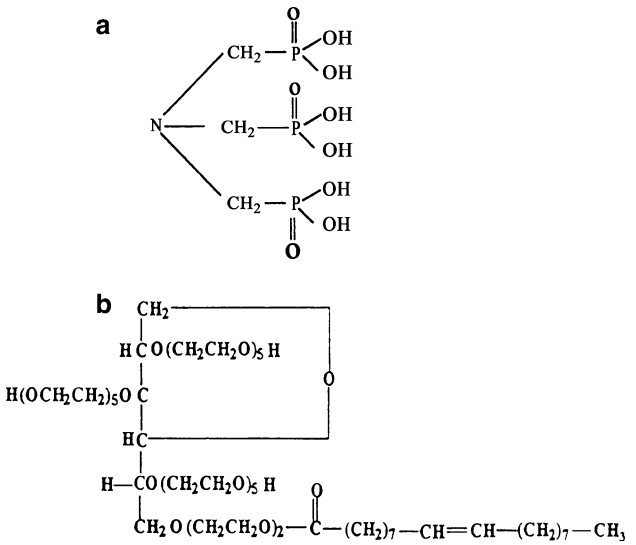


**Fig. 1** The structure of inhibitor compounds (**a**) aminotrimethylidene phosphonic acid and (**b**) Tween 80

The working electrode was depolarised to –1100 mV for 1 min to remove the native oxides on the surface and was allowed to stabilize for an hour until a constant potential was reached; this is referred to as the corrosion potential ($E_{corr}$). The cathodic and anodic polarization curves for 304 SS specimen in the test environment were recorded at a sweep rate of 1 $mV\ s^{-1}$. In all the cases the potential was changed in the cathodic direction from the corrosion potential to –1200 mV and the electrode was left to attain the corrosion potential. Then the electrode was anodically polarized up to 1600 mV. All the electrochemical experiments were carried in nitrogen atmosphere by purging with nitrogen gas.

#### *2.1.4 Electrochemical impedance studies*

Electrochemical impedance studies were carried out using Solartron SI 1285 electrochemical interface controlled by commercial software.

### 2.2 Surface characterization studies

The 304 SS specimens were immersed in blank, as well as inhibitor solutions, for a period of 30 days. After 30 days, the specimens were taken out and dried. The nature of the film formed on the surface of the metal specimens was analyzed by various surface analysis techniques.

#### *2.2.1 Luminescence spectra*

Luminescence spectra of the films formed were recorded using a Perkin-Elmer LS5B fluorescence

spectrophotometer equipped with a pulsed Xenon lamp, attached to an IBM PC via an RS-232C interface. The emission spectra were corrected for the spectral response of the photomultiplier tube used.

#### 2.2.2 FTIR spectra

The FTIR spectra were recorded using a Perkin-Elmer 1600 FTIR spectrophotometer.

#### 2.2.3 X-ray diffraction technique

XRD patterns of the film formed on the metal surface were recorded using a computer controlled Rigaku-Denki RU 200 diffractometer with $CuK_\alpha$ (Ni-filtered) radiation ($\lambda$ = 1.5418) at a rating of 40 kV, 20 mA. The scan rate was 0.05-20° per step and measuring time was 1 s per step.

#### 2.2.4 XPS studies

The surface analysis of the passive films using XPS was carried out to understand the nature and composition of the passive films in the presence and absence of inhibitors. Each electrode was immersed in groundwater in the absence and presence of the optimum concentration of inhibitor, and a current of 1.5 mA $cm^{-2}$ was applied to the cathodic direction for 15 min to reduce the oxides. Then the specimens kept under open circuit potential for 1 h to the film to grow. At the end of the experiment the specimens were removed, washed with deionized water, dried using purified argon and stored in an airtight desiccator until they were used for XPS analysis.

The XPS analysis was performed with VG ESCA LAB Mark II spectrometer using an Al $K_\alpha$ X-ray source with a mean kinetic energy of 1486.6 eV. All the experiments were carried out at a vacuum of $10^{-7}$–$10^{-9}$ torr. The output of the photoelectron analysis was obtained as binding energy versus intensity counts. The high-resolution spectra were taken for O 1s, Fe 3s, N 1s electrons. The profile analysis was made with an argon ion pressure of 20 mPa, an applied voltage of 4.5 kV and a current of 25 $\mu$A for 9 min.

The binding energy of the inhibited surface was measured from the spectra obtained for the respective elements and then the values were corrected with respect to the reference C 1s binding energy value. Data reduction was carried out by deconvoluting the high-resolution composite XPS peaks of the individual species of different oxidation states. This was done using ORIGIN software.

#### 2.2.5 Scanning Electron Microscopic studies (SEM)

After polarization measurements, the electrode was removed from the cell, thoroughly washed with distilled water, cleaned with acetone, dried and observed in a scanning electron microscope to examine pit morphology. The metallographic examinations of the 304 SS were carried out using a Leica Stereoscan 440 computer controlled scanning electron microscope.

## 3 Results and discussion

### 3.1 Electrochemical techniques

#### 3.1.1 Open circuit potential—time measurement

Table 2 gives the data of OCP—time measurements for 304 SS in groundwater containing various inhibitor systems. It is clear that the presence of ATMP, shifted the OCP value in the noble (positive) direction i.e., –6 mV, indicating that the inhibitor controls the anodic reaction. In the presence of $Zn^{2+}$ the OCP value was found to be –187 mV, indicating that it controls the cathodic reaction. Similarly the presence of Tween 80 also shifted the OCP value in the noble region (–72 mV). The combination of ATMP (30 ppm) and $Zn^{2+}$ (50 ppm) shifted the OCP value to –20 mV thereby indicating that this combination controls both the cathodic and the anodic reaction. With the addition of Tween 80 to the above mixture, the OCP value was shifted to –4 mV indicating that this combination predominantly controls the anodic dissolution of the metals by forming a protective film which is responsible for the minor variations observed in the curves.

#### 3.1.2 Polarization measurement

The cathodic and anodic polarization of 304 SS in groundwater in the presence and absence of various concentration of the inhibitor were carried out. Each inhibitor was studied at eight different concentration levels. In the case of ATMP the inhibition efficiency was found to increase appreciably with increase in inhibitor concentration up to 30 ppm, after which it decreased. Similarly the optimum concentration of $Zn^{2+}$ and Tween 80 were also evaluated based on inhibition efficiency and were found to be 50 and 150 ppm, respectively.

The polarization curve data of ATMP are shown in Table 2. The corrosion potential ($E_{corr}$) of 304 SS shifted in the noble direction and a decrease in $I_{corr}$ was

**Table 2** Polarization parameters of 304 SS in groundwater in the presence of combination of inhibitors

| Inhibitor | Concentration/ppm | OCP/mV | $E_{corr}$/mV | $I_{corr}$ × $10^{-2}$/mA $cm^{-2}$ | $E_b$/mV | IE/% | Synergism (*s*) |
|---|---|---|---|---|---|---|---|
| Blank | – | –171 | –76 | 1.000 | 790 | – | – |
| $Zn^{2+}$ | 50 | –187 | –70 | 0.370 | 800 | 63.0 | – |
| ATMP | 30 | –006 | –01 | 0.250 | 958 | 75.0 | – |
| Tween 80 | 150 | –072 | –14 | 0.500 | 908 | 50.0 | – |
| $Zn^{2+}$ + ATMP | 50 + 30 | –020 | –10 | 0.062 | 1056 | 93.8 | 1.49 |
| $Zn^{2+}$ + ATMP + Tween 80 | 50 + 30 + 150 | –004 | –27 | 0.010 | 1095 | 99.0 | 3.10 |

IE – Inhibition efficiency

noticed with the addition of ATMP. In the presence of $Zn^{2+}$, the polarization data were shifted towards the region of lower current density ($I_{corr}$). From the polarization curves it can be inferred that $Zn(OH)_2$ formed on the metal surface retards the oxygen reduction reaction and thus controls the cathodic reaction of the metal. However, the combination consisting of 30 ppm of ATMP and 50 ppm of $Zn^{2+}$, reduced $I_{corr}$ to 0.062 × $10^{-2}$ mA $cm^{-2}$ and also the breakdown potential ($E_b$) was shifted in the noble direction, indicating that the dissolution of the metal was reduced. There was a further decrease in $I_{corr}$ with the addition of 150 ppm of Tween 80. Thus a powerful synergism was exhibited by the combination of these inhibitors in ground water. The observed synergism may be related to either interaction between the inhibitor compounds or interaction between the inhibitor compounds and one of the ions present in the aqueous medium.

The synergism '*s*' was calculated using the formula [38] $s = (i_1 i_2)/(i_{1,2} i_0)$ where, $i_1$, $i_2$, $i_{1,2,}$ are the current densities associated with the additives 1, 2 and 1 + 2, respectively; $i_0$ is the current density for the blank solution. In the case of ternary system, $i_1$, $i_2$, $i_{1,2,}$ represents the current densities corresponding to the additives 1 + 2, 3 and 1 + 2 + 3.

*s* approaches 1 when no interaction between the inhibitor compounds exists. When $s > 1$, this points to synergistic effects. In the case of <1, the negative interaction of inhibitors prevails (i.e., corrosion rate increases).

The mechanistic aspects of the inhibition of 304 SS in groundwater by ATMP, $Zn^{2+}$ and Tween 80 can be explained in terms of complexation and adsorption. $Zn^{2+}$ and phosphonic acid are able to form complexes with iron surface. During the dissolution of iron, the pH increases at the metal/electrolyte interface due to oxygen reduction. Thus $Zn(OH)_2$ precipitation may take place at cathodic sites [7, 8] thus decreasing the rate of further oxygen reduction.

Addition of phosphonic acids (PA) reduces metal dissolution; this may be due to adsorption and complex formation at the surface [7–11, 39, 40]. With the combined application of $Zn^{2+}$ and ATMP, the corresponding anodic and cathodic reactions of the metal can be generalized as follows. The local cathodic region was inhibited by $Zn^{2+}$ ion and the local anodic region was inhibited by ATMP. The Zn–PA complex diffuses from the bulk solution to the surface of the metal and is converted into a Fe–PA complex, which is more stable than Zn–PA [8]. The released $Zn^{2+}$ causes $Zn(OH)_2$ precipitation at the local cathodic sites. Thus the protective film consists of an Fe–PA complex and $Zn(OH)_2$. The presence of Tween 80 induces hydrophobicity and may favor inhibitor dispersibility and limit corrosion, which is evident from the increased inhibition efficiency.

### 3.1.3 *Electrochemical impedance studies*

The impedance plots of 304 SS in groundwater with various inhibitors are presented in Fig. 2. The EIS parameters are given in Table 3. An increase in polarization resistance and a decrease in capacitance with the addition of $Zn^{2+}$ to ATMP shows better corrosion resistance. The decrease in capacitance is due to the increase in complex formation at the metal interface.

A significant synergistic effect was achieved by the addition of the non-ionic surfactant Tween 80 to the $Zn^{2+}$ + ATMP system. It can be postulated that the long hydrocarbon part of Tween 80 ensures large surface coverage. If the alkyl group is too long, the hydrophobicity of the molecule increases which promotes the surface activity of the molecule, thus accounting for a considerable increase in $E_b$. Thus the addition of a surfactant to the $Zn^{2+}$ + ATMP system provides an effective impervious barrier to the dissolution of metal and thus affords corrosion protection.

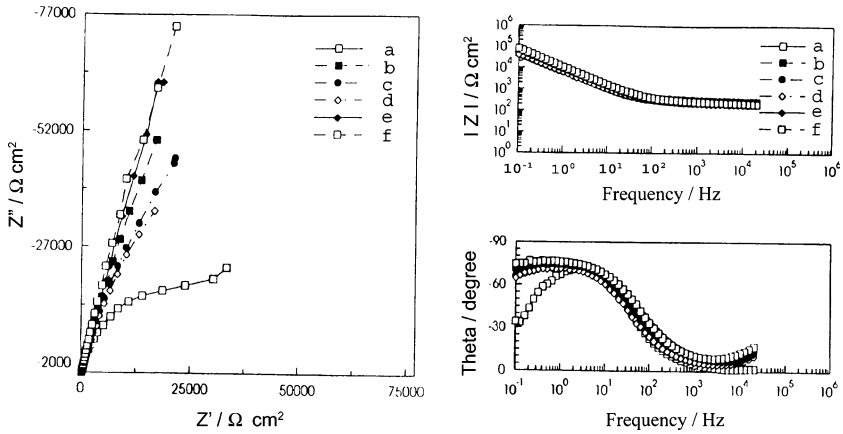


**Fig. 2** Nyquist and Bode plot of 304 SS at different concentration ratios of inhibitors in groundwater. (**a**) Blank, (**b**) ATMP, (**c**) $Zn^{2+}$, (**d**) Tween 80, (**e**) $Zn^{2+}$ + ATMP (f) $Zn^{2+}$ + ATMP + Tween 80

**Table 3** Impedance parameters of 304 SS in the presence of different inhibitor mixture in groundwater

| Inhibitors | Concentration/ppm | Polarisation resistance $\times$ $10^2$/kΩ $cm^{-2}$ | Capacitance/$\mu$F $cm^{-2}$ |
|---|---|---|---|
| Blank | – | 57.38 | 81.68 |
| $Zn^{2+}$ | 50 | 198.25 | 77.81 |
| ATMP | 30 | 325.30 | 67.70 |
| Tween 80 | 150 | 152.32 | 79.99 |
| $Zn^2$ + ATMP | 50+30 | 788.05 | 59.32 |
| $Zn^2$ + ATMP + Tween 80 | 50 + 30 + 150 | 3932.05 | 35.10 |

## 3.2 Surface characterization

### *3.2.1 Luminescence spectra*

The UV-luminescence emission spectra of the solid Fe–ATMP complex excited at 360 nm is shown in Fig. 3. The luminescence spectra of the films formed on the surface of the metal specimen immersed for a period of 30 days in ATMP, ATMP + $Zn^{2+}$ and ATMP + $Zn^{2+}$ + Tween 80 were recorded using an exciting wave length of 360 nm (Fig. 4). The intensity of the luminescence spectra of the film formed from ATMP alone is weak compared to that of ATMP + $Zn^{2+}$ and ATMP + $Zn^{2+}$ + Tween 80 systems. It has been postulated that several oxides of iron are formed on the metal surface [8–10]. The composition of iron oxides minimizes the formation of complex between Fe and ATMP and therefore the intensity of the luminescence spectrum is found to be very weak (Fig. 4a). In the presence of ATMP + $Zn^{2+}$ and ATMP + $Zn^{2+}$ + Tween 80, 93.8% and 99.0% inhibition efficiency was achieved, respectively, due to Fe–ATMP complex formation which also accounts for the increase in intensity of the luminescence spectra (Fig. 4b, c).

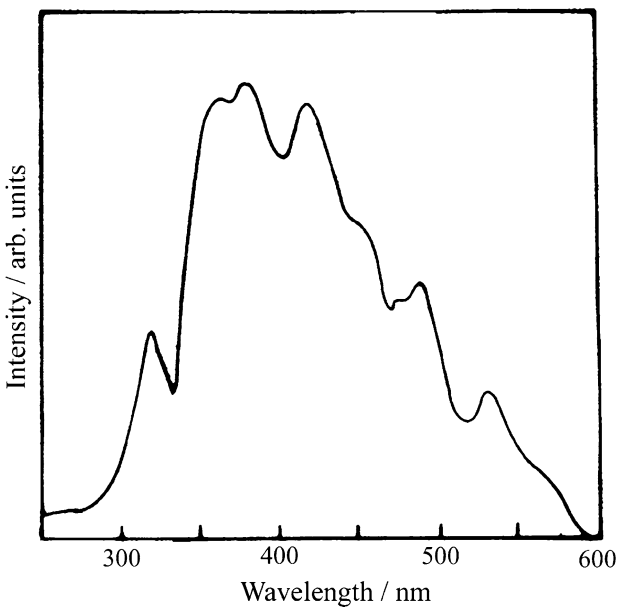


**Fig. 3** Luminescence emission spectra of solid Fe–ATMP complex at $\lambda_{ex}$ = 360 nm

### *3.2.2 Fourier Transform-Infrared spectra (FTIR-spectra)*

The FTIR Spectrum of ATMP is shown in Fig. 5. The FTIR reflection spectrum of the ATMP and surface passive film formed on 304 SS was recorded. The results are shown in Fig. 6.

A characteristic feature of the ATMP molecule is the prominent presence of the C–N absorption band.

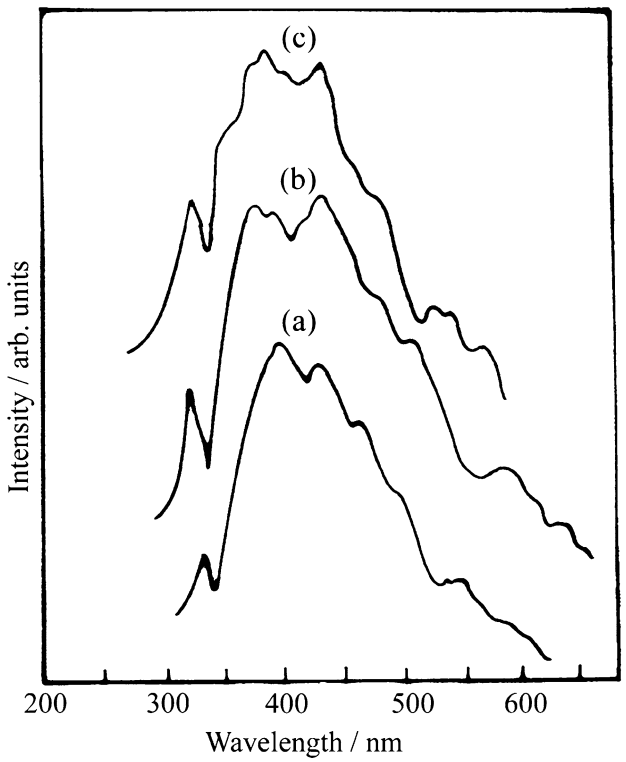


**Fig. 4** Luminescence emission spectra of the surface film formed on 304 SS in groundwater media at $\lambda_{ex}$ = 360 nm. (**a**) ATMP, (**b**) ATMP + $Zn^{2+}$ and (c) $Zn^{2+}$ + ATMP + Tween 80

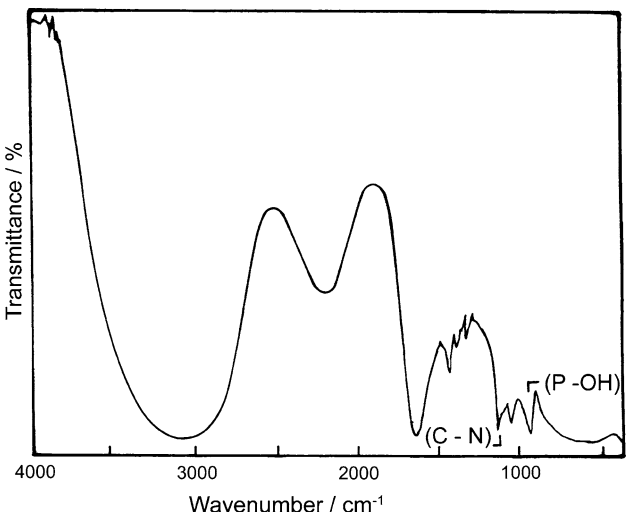


**Fig. 5** Infrared transmission spectra of ATMP

The peak at 1145 $cm^{-1}$ is attributed to the C–N absorption band while the peak at 1102 $cm^{-1}$ is due to the P–O band. In the case of immersed test samples, the C–N and P–OH were observed at 1105 and 930 $cm^{-1}$, respectively. This is probably due to the decrease in electron cloud density of the C–N and P–O

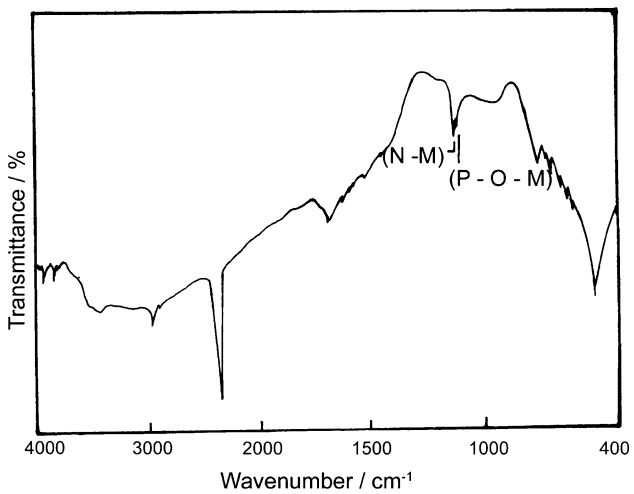


**Fig. 6** Infrared reflection–absorption spectrum of the film formed on the 304 SS substrate after immersion in the solution containing the mixture of ATMP + $Zn^{2+}$ + Tween 80

bands due to the shift of electron cloud density from N and O atoms to $Fe^{2+}$. As previously mentioned, the corrosion inhibition of steel by $Zn^{2+}$ is due to the formation of $Zn(OH)_2$ [41]. The band around 850 $cm^{-1}$ may be assigned to the Zn–OH bending mode. The substitution of an OH group by a halogen shifts the Zn–OH bending mode to lower frequency. Nevertheless, the presence of different bands in the region 780–850 $cm^{-1}$ suggests the formation of compounds of complex structure such as $Zn_x(OH)_y$ $(Cl)_z$ [41].

### *3.2.3 X-ray Diffraction Technique (XRD)*

The X-ray diffraction patterns of the surface film of the SS specimens immersed in various test solutions is given in Fig. 7. The peak due to iron appears at $2\theta$ = 44.3° and 65.3°. Peaks at $2\theta$ = 30.4°, 36° and 62.4° can be assigned to oxides of iron. Thus, it is observed that the surface of the metal immersed in groundwater contains $Fe_3O_4$[42]. This indicates that in groundwater the 304 SS specimen has undergone corrosion leading to the formation of magnetite.

The XRD pattern for the sample immersed in solution containing 30 ppm of ATMP + 50 ppm of $Zn^{2+}$ are given in Fig. 7b. The peak due to iron occurs at $2\theta$ = 44.4° and 64.9°. The peaks corresponding to Γ-FeOOH appear at $2\theta$ = 36.9° and 61.5° [42]. The XRD pattern of the surface immersed in solution containing 30 ppm ATMP + 50 ppm $Zn^{2+}$ + 150 pmm Tween 80 is given in Fig. 7c. The peaks due to oxides of iron such as $Fe_3O_4$, and Γ-FeOOH are absent and peaks due to iron alone are observed at $2\theta$ = 44.4° and 64.9°.

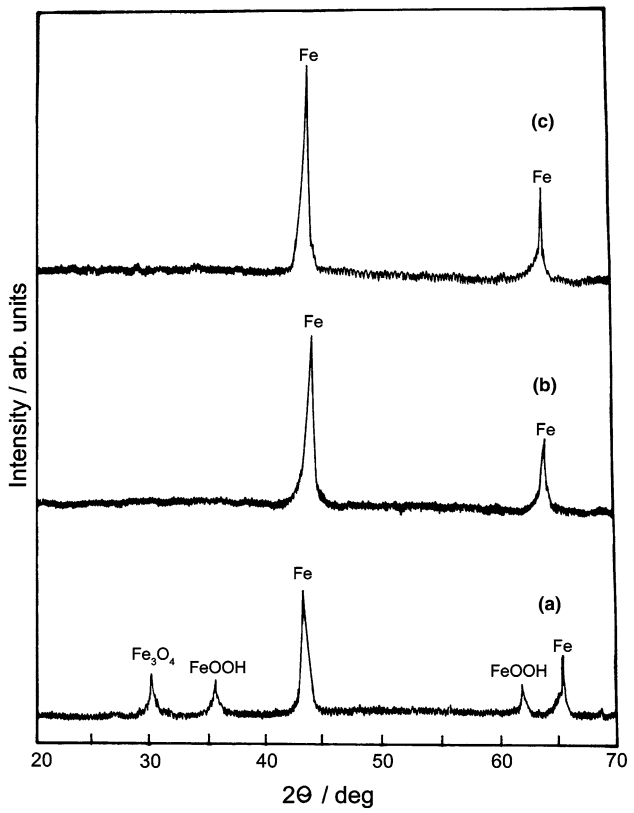


**Fig. 7** XRD pattern obtained on the surface film formed on 304 SS at the end of 30 days in different environment. (**a**) Blank, (**b**) $Zn^{2+}$ + ATMP and (**c**) $Zn^{2+}$ + ATMP + Tween 80

### 3.2.4 *X-ray Photoelectron Spectroscopy (XPS)*

During passivation, surface enrichment of alloy components, monolayer formation and chemical states of the film constituents can be investigated by surface sensitive techniques [43–48]. XPS have been utilised to study the chemical nature of the interface between inhibitor and metal substrates.

*3.2.4.1 Iron spectra* XPS analysis was carried out in the binding energy ranging from 690 to 740 eV in order to elucidate the presence of iron components and their oxidation states at the blank and inhibited surfaces. The deconvoluted high-resolution spectra Fe $P_{3/2}$ are illustrated in Fig. 8.

Iron $P_{3/2}$ energy level spectra, on deconvolution, yielded three peaks at binding energy values of 706.8, 709.1, and 711.3 eV for Fe, $Fe^{2+}$ and $Fe^{3+}$, respectively (Fig. 8a). On argon sputtering, the composition of both the possible oxide species, FeO and FeOOH decreased (Fig. 8b), while the metal contribution increased from just 20% to 40% indicating that oxides of iron are present in the outermost layers of the passive film.

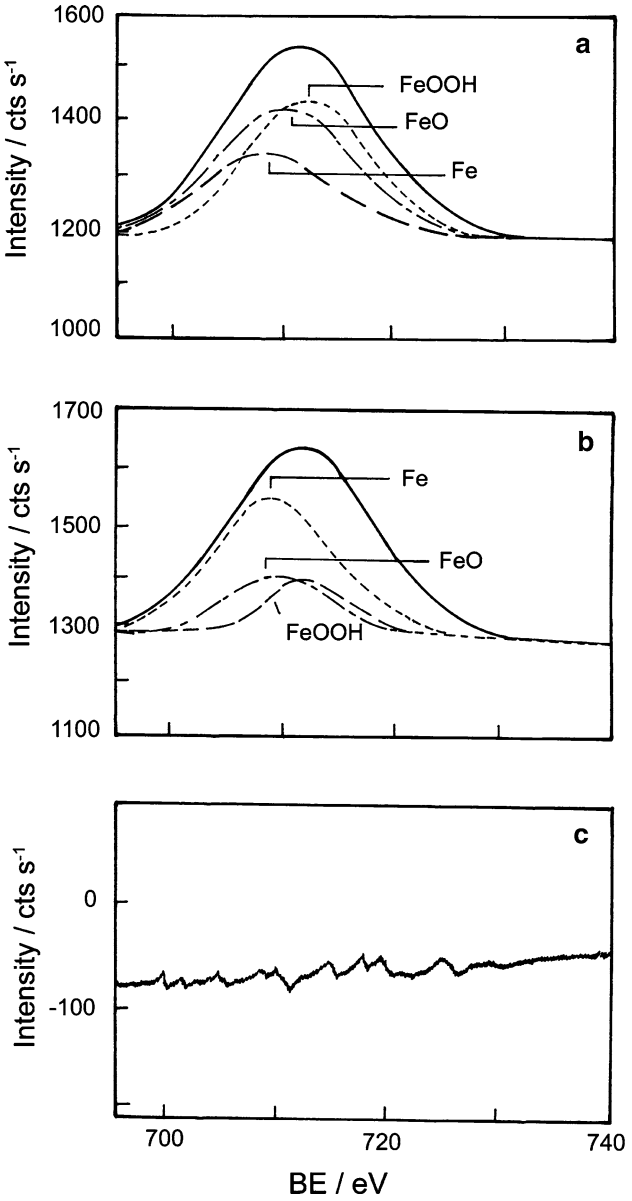


**Fig. 8** High resolution XPS spectra of iron in the passive film of (**a**) passivated surface (**b**) sputtered surface and (**c**) inhibited with ATMP + $Zn^{2+}$ + Tween 80 surface for 304 SS in groundwater media

Several studies have reported that iron in the above oxide forms exhibits similar binding energy values when present in the passive film [49, 50]. The amount of metallic iron and oxides of iron almost completely vanish with the addition of the optimum concentration of ATMP + $Zn^{2+}$ + Tween 80 (Fig. 8c).

*3.2.4.2 Chromium spectra* The high-resolution photoelectron spectra of Cr 2 $P_{3/2}$ energy level was recorded in the binding energy window 475–600 eV for

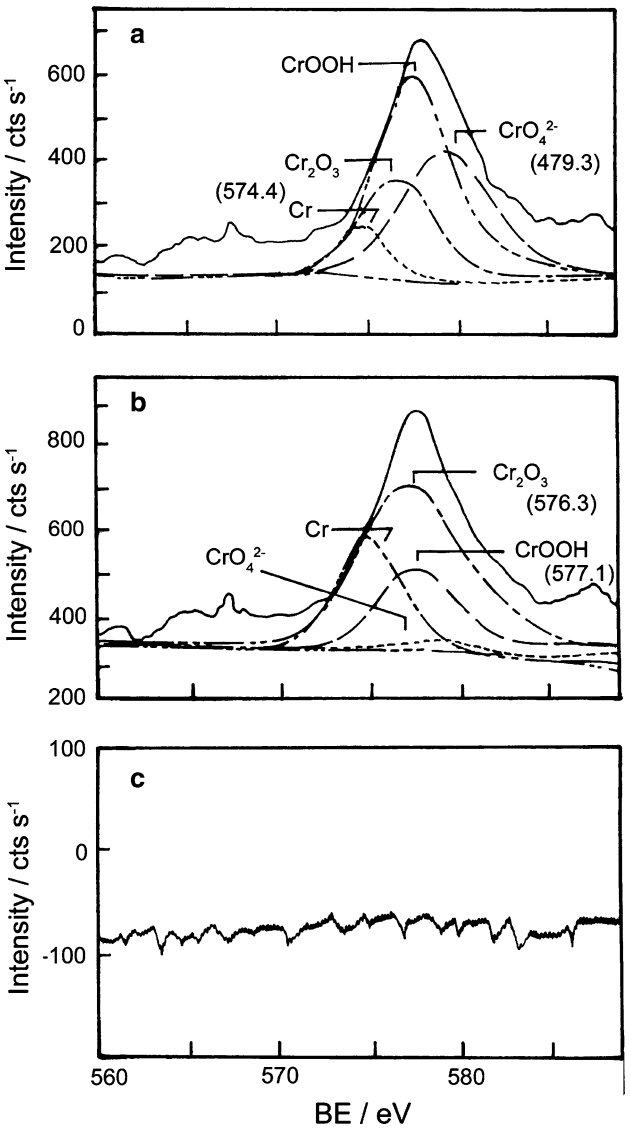


**Fig. 9** High resolution XPS spectra of chromium in the passive film of (**a**) passivated surface, (**b**) sputtered surface and (**c**) inhibited with ATMP + $Zn^{2+}$ + Tween 80 surface for 304 SS in groundwater media

the blank and inhibited surfaces. Groundwater was (without addition of inhibitor) considered as a base line solution for the study. Figure 9 illustrates the high-resolution XPS spectra of chromium Cr 2 $P_{3/2}$ energy level for 304 SS yielded four peaks. The peaks at binding energy values of 576.3, 577.1 and 579.3 eV correspond to $Cr_2O_3$, $CrOOH/Cr(OH)_3$ and $CrO_4^{2-}$, respectively. The metal peak at binding energy value of 574.4 eV is very small in comparison with the amplitude of other peaks (Fig. 9a). The intensity of these compounds is in the order $CrOOH/Cr(OH)_3$ > - $CrO_4^{2-}$ > $Cr_2O_3$ >> Cr. This indicates that the outermost layer of the passive film contains $Cr(OH)_3$ as the major constituent as reported by Brooks et al. [51].

On argon sputtering, the intensity of the Cr $2P_{3/2}$ energy levels was increased. The feature changes are the enrichment of the $Cr_2O_3$ phase at the inner layer (Fig. 9b) and almost complete vanishing of the $CrO_4^{2-}$ peak. The intensity of $Cr_2O_3$ peak increases (25% of $Cr_2O_3$ in the inner layer) on ion sputtering indicating that $Cr_2O_3$ is present in the inner layers i.e., at the metal–oxide interface. The ratio of $Cr(OH)_3$ and $CrO_4^{2-}$ intensity to total chromium intensity decreases, indicating that the outermost layer contains higher amounts of $Cr(OH)_3$ and $CrO_4^{2-}$.

In all the above cases, chromium was found as $Cr^{3+}$ and $Cr^{6+}$ in the various forms of oxide and hydroxides at their respective binding energy values, which is in agreement with earlier work [51, 52]. The amount of chromium in metallic and oxide form almost completely vanish with the addition of the optimum concentration of ternary inhibitor (Fig. 9c).

*3.2.4.3 Oxygen spectra* Three types of chemical states of oxygen can be distinguished in the altering shape of the O 1s line related to the O–Fe (530.2 eV), OH–Fe (531.4 eV), O–P (532.3 eV) and adsorbed $H_2O$ (533.2 eV) from the environment (Fig. 10a). After argon sputtering, the water molecule peak was decreased, as depicted in Fig. 10b. The O–P peak was observed with the addition of optimum concentration of phosphonic acid (ATMP), while the concentration of Fe–O and Fe–OH decreased simultaneously as shown in Fig. 10b.

With the addition of $Zn^{2+}$ along with the ATMP, a rapid decrease of the Fe 2p-signal intensity was observed [50] (Fig. 10c). These observations, together with the simultaneous increase of the phosphorous signal, are consistent with growing inhibitor layer thickness at this concentration ratio.

*3.2.4.4 Nitrogen spectra* Inhibited and uninhibited specimens were scanned between 350 and 450 eV to study the nitrogen present in the surface of the metal. The deconvoluted high resolution spectra are illustrated in Fig. 11.

The nitrogen spectrum for inhibited surface of 304 SS is shown in Fig. 11b, the main peak at 401.6 eV corresponding to Fe–N. There is no peak corresponding to nitrogen on uninhibited surface (Fig. 11a). A very weak signal for nitrogen with a count rate less than 150 cts $s^{-1}$ is observed for the inhibited surface,

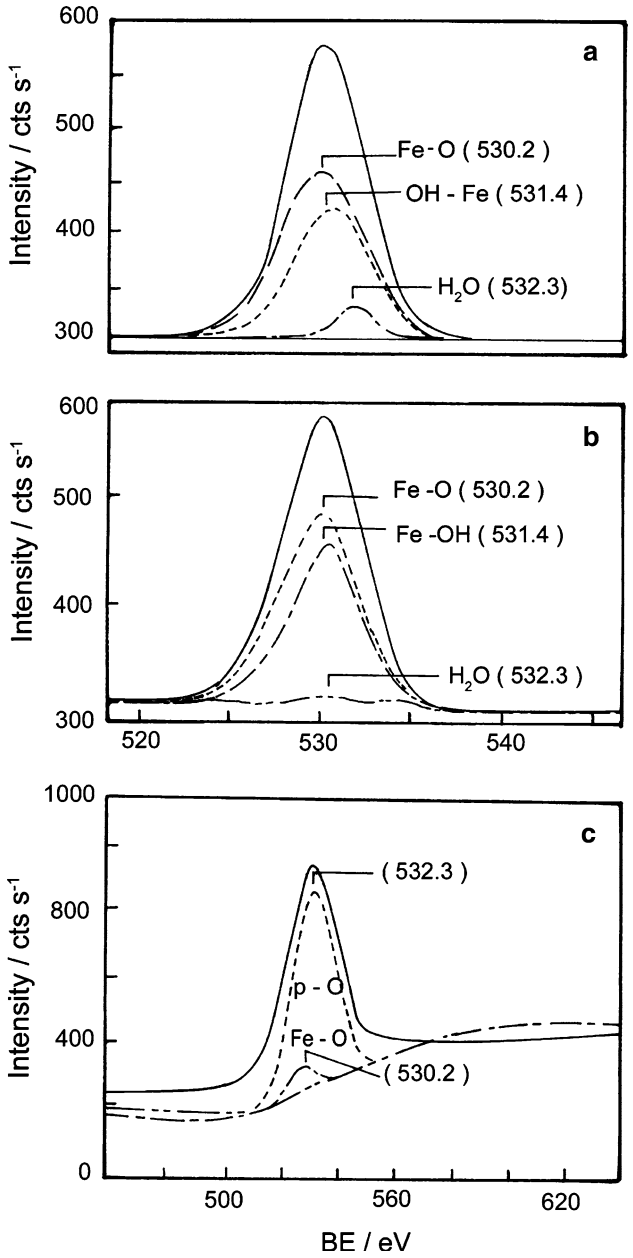


**Fig. 10** High resolution XPS spectra of oxygen in the passive film of (**a**) passivated surface (**b**) sputtered surface and (**c**) inhibited with ATMP + $Zn^{2+}$ + Tween 80 surface for 304 SS in groundwater media

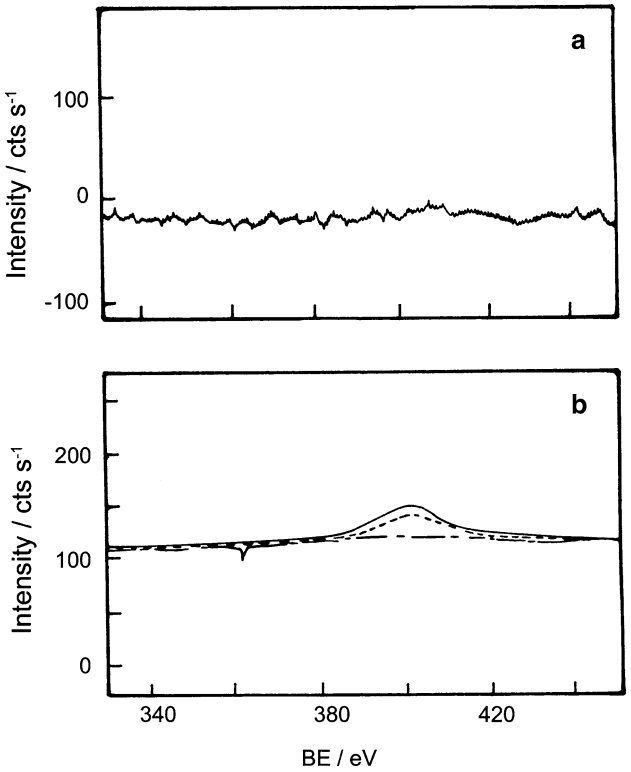


**Fig. 11** High resolution XPS spectra of nitrogen in the passive film of (**a**) passivated surface and (**b**) inhibited with ATMP + $Zn^{2+}$ + Tween 80 surface for 304 SS in groundwater media

this confirms the formation of protective passive film on the metal surface obviously due to the small contribution of nitrogen in the inhibitor molecule. Thus, the XPS studies of the passive film are useful to predict the exact role played by the inhibitor in aiding the stability of the passive film which in turn, accounts for the improved corrosion resistance. In all the inhibited cases, the counts of Cr, O, Fe and N are nearly constant after 10 min of $Ar^{2+}$ sputtering, which indicates that the passive film is homogeneous [53, 54].

### 3.2.5 SEM studies

To understand the nature of the surface film in the absence and presence of inhibitors and the extent of corrosion of 304 SS, the micrographs of the surface after polarisation measurement are examined. The size, number and distribution of pits over the metal surface give a rough estimation of the stainless steel resistance towards pitting attack. Although the initiation and growth of the pits largely depend upon the environment, the inhibitor combination played a major role.

The higher magnification of the pits on 304 SS is carried out by SEM studies (Fig. 12). The SEM micrograph (Fig. 12a) focuses a single pit whose diameter is around 3 $\mu$m. In the presence of inhibitor system, the pit was smaller even under the high magnification shown in (Fig. 12b). The higher $E_b$ potential observed in this inhibitor substantially supports the

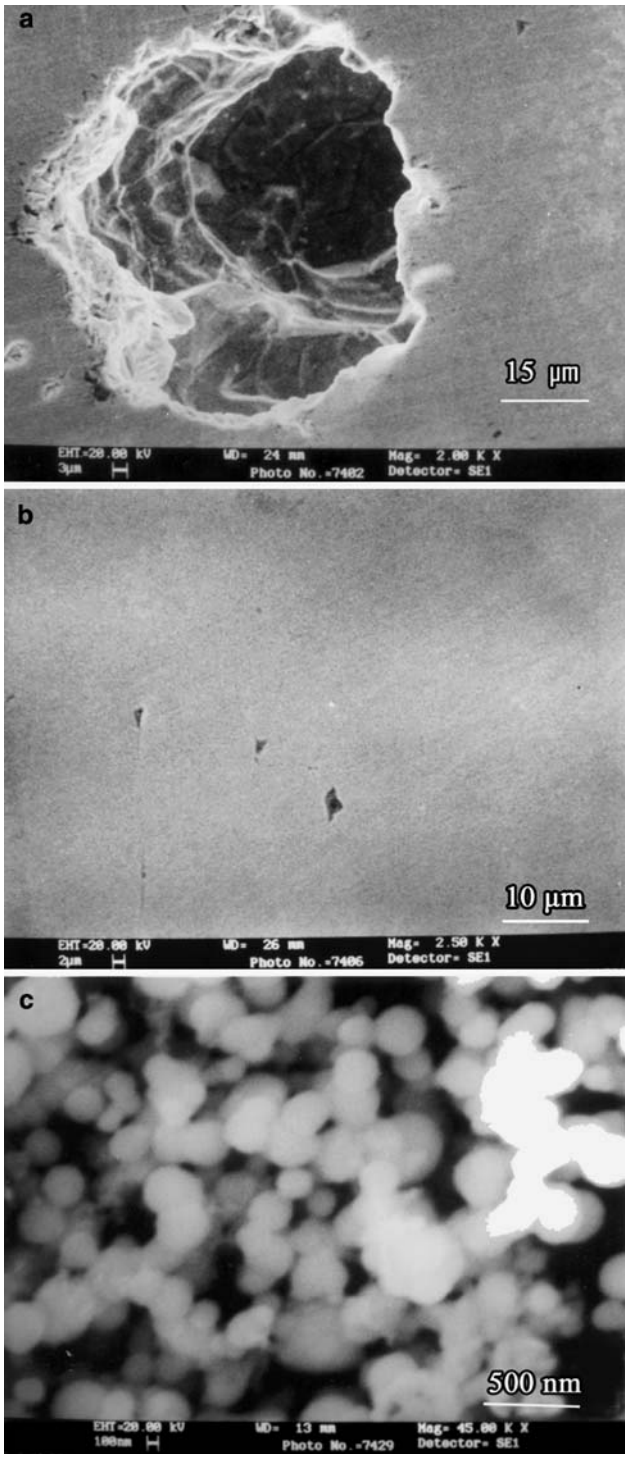


**Fig. 12** Scanning Electron Micrographs (SEM) of 304 SS (**a**) uninhibited surface (**b**) inhibited surface (**c**) complex formation of ATMP + $Zn^{2+}$ + Tween 80

evidence for this observation. This is mainly due to the formation of complex on the surface of the metal.

Among the various combination of inhibitor system, ATMP + $Zn^{2+}$ + Tween 80 combination is chosen for SEM studies because of its best inhibition efficiency for 304 SS as evident from the electrochemical and surface analytical measurements. Figure 12c indicated that in the presence of ATMP + $Zn^{2+}$ + Tween 80 mixture, the surface coverage increases which in turn results in the formation of insoluble complex on the surface of the metal. In the presence of ATMP + $Zn^{2+}$ + Tween 80, the surface is covered by a thick layer of inhibitors which effectively control the dissolution of 304 SS.

## 4 Conclusion

A formulation consisting of $Zn^{2+}$, ATMP and Tween 80 can be used as a potent inhibitor to prevent the pitting corrosion attack of 304 SS in ground water media.

- Significant synergism was attained by the combined application of ATMP, $Zn^{2+}$ and Tween 80 of 0.3: 0.5: 1.5 ratio.
- The concentration dependence of inhibition efficiency were found to be the same for both ac and dc measurements.
- Surface analytical studies such as luminescence spectra, FTIR, XRD, XPS and SEM studies revealed that the film is composed essentially of iron phosphonate complex.
- Electrochemical measurements coupled with surface analytical techniques proved to be effective means of characterizing the enhanced inhibitive effect of phosphonic acid and $Zn^{2+}$ along with surfactants on the corrosion of 304 SS in aqueous media.

## References

1. Dugdale I, Cotton JB (1963) Corros Sci 3:69
2. Poling CW (1980) Corros Sci 10:887
3. Walker R (1973) Corrosion 29:290
4. Gopi D, Bhuvaneswaran N, Rajeswari S, Ramadas K (2000) Anti-Corrosion Methods Mater 47:332
5. Schmitt G (1984) Br Corros J 19:165
6. Trabanelli G (1991) Corrosion 47:410
7. Gopi D, Bhuvaneswaran N, Rajeswari S (2002) Bull Electrochem 18:29
8. Gopi D, Rajeswari S (2002) J Solid State Electrochem 6:194
9. Gopi D, Rajeswari S (2001) Proc international conference on advances in surface science and engineering (INSURE), Chennai, India, 21–23 Feb, pp 210
10. Gopi D, Rajeswari S (2000) Proc NACE international conf, corrosion its mitigation and preventive maintenance, Mumbai, India, 20–23 Nov, vol 1, pp 435
11. Gopi D, Rajeswari S (2000) Proc tenth national congress on corrosion control, conf, Madurai, India, 6–8 Sep, pp 353

12. Latha G, Rajeswari S (1996) Anti-Corrosion Methods Mater 43:19
13. Lu KH, Duquette DJ (1990) Corrosion 46:994
14. Latha G, Rajeswari S (2000) Corrosion Rev 18:429
15. Babic R, Metikos-Hukovic M, Loncar M (1999) Electrochim Acta 44:2413
16. Zhong S, Wang I, Liu HK, Dou SX (1999) J Appl Electrochem 29:177
17. Guzman RSS, Vilche JR, Arvia AJ (1979) Electrochim Acta 24:395
18. Drazic DM, Hao CS (1982) Electrochim Acta 27:1409
19. MacDonald DD, Owen D (1973) J Electrochem Soc 120:317
20. Zhang H, Park SM (1994) J Electrochem Soc 141:718
21. Galvele JR (2005) Corros Sci 47:3053
22. Dagbert C, Meylheuc T, Bellon-Fontaine M-N (2006) Electrochim Acta 51:5221
23. Alamr A, Bahr DF, Jacroux M (2006) Corros Sci 48:925
24. Cosman NP, Fatih K, Roscoe SG (2005) J Electroanal Chem 574:261
25. Yang W, Zhao G, Zhang M, Congleton J (1992) Corros Sci 33:89
26. Hirano H, Aoki N, Kurosawa T (1983) Corrosion 39:313
27. Congleton J, Zheng W, Hua H (1990) Corros Sci 30:555
28. Ibach H (ed) (1977) Electron spectroscopy for surface analysis. Springer-Verlag, Heidelberg, Germany
29. Brundle CR (1978) Surf Sci 48:99
30. Batina N, Caffins SA, Kahn BE, Lu F, McCarger JW, Rovang JW, Stern DA, Hubbard AT (1989) Catal Lett 3:275
31. Kirchheim R, Heine B, Fischmeister H, Hofmann S, Knote H, Stolz U (1989) Corros Sci 29:899
32. Gui J, Devine TM (1991) Corros Sci 32:1105
33. Hara N, Sugimoto K (1979) J Electrochem Soc 126:1328
34. Mc Bee CL, Kruger J (1972) Electrochim Acta 17:1337
35. Haupt S, Strehblow HH (1995) J Electrochem Soc 37:43
36. Schmuki P, Virtanen S (1997) Interface 6:41
37. Schmuki P, Virtanen S (2001) J Appl Electrochem 31:913
38. Felhosi I, Keresztes Zs, Karman FH, Mohai M, Bertoti I, Kalman E (1999) J Electrochem Soc 146:961
39. Veres A, Reinhard G, Kalman E (1992) Br Corros J 27:147
40. Kalman E (1994) Corrosion inhibitors, Published for EFC No. 11, Institute of Materials London
41. Srivastava OK, Secco EA (1967) Can J Chem 45:585
42. Favre M, Landolt D (1993) Corros Sci 34:1481
43. Patterson TA, Carver JC, Leyden DE, Hercules DM (1976) J Phys Chem 80:1700
44. Mischler S, Vogel A, Mathieu HJ, Landolt D (1991) Corros Sci 32:925
45. Bardwell JA (1990) Corros Sci 30:1009
46. Hara N, Sugimoto K (1979) J Electrochem Soc 126:1328
47. Bundle CR, Roberts MW (1973) Chem Phys Letters 18:380
48. Bundle CR, Carley AF (1975) Faraday Discussions 60:51
49. Stout DA, Lumsden JB, Stachle RW (1979) Corrosion 35:141
50. Mclntyre NS, Zetaruk DG (1977) Anal Chem 49:1521
51. Brooks AR, Clayton CR, Doss K, Lu YC (1986) J Electrochem Soc 133:2459
52. Karman FH, Felhosi I, Kalman E, Cserny Kover I (1998) Electrochim Acta 43:69
53. Fang JL, Li Y, Ye XR, Wang ZW, Liu Q (1993) Corrosion 49:266
54. Wagner CD, Riggs WM, Davis LE, Moulder JF, Mullenberg GE (1978) In: Praine MN (ed) Handbook of X-ray photoelectron spectroscopy. Perkin-Elmer Corp